

Hybrid Visual Servoing Tracking Control of Uncalibrated Robotic Systems for Dynamic Dwarf Culture Orchards Harvest

Tao Li¹ and Quan Qiu¹ and Chunjiang Zhao¹

Abstract—The paper is concerned with the dynamic tracking problem of SNAP orchards harvesting robots in the presence of multiple uncalibrated model parameters in the application of dwarf culture orchards harvest. A new hybrid visual servoing adaptive tracking controller and three adaptive laws are proposed to guarantee harvesting robots to finish the dynamic harvesting task and the adaption to unknown parameters including camera intrinsic and extrinsic model and robot dynamics. By the Lyapunov theory, asymptotic convergence of the closed-loop system with the proposed control scheme is rigorously proven. Experimental and simulation results have been conducted to verify the performance of the proposed control scheme. The results demonstrate its effectiveness and superiority.

I. INTRODUCTION

In fresh fruit production, harvesting is one of the most labor-intensive operations incurring the high cost, and often depends on a large seasonal workforce, which is becoming less available. Harvesting robots are expected to cope with the non-customized and unstructured orchard working environment that is very different from industrial robots. In the past years, many investigators have carried out manifold mechanisms and control strategies of robots to handle the complicated working environment [1]–[3]. Despite the fruitful achievements, the performance of harvesting robots in the unstructured orchards is still unsatisfactory.

Nowadays, an increasing number of orchards are employing modern agricultural strategies, high-density dwarf planting, where the fruiterers are SNAP (Simple, Narrow, Accessible, and Productive) tree architectures and form "fruiting walls". The working environment of robots is consequently simplified, bringing considerable convenience to robots as well as humans in harvest operation. Recently, SNAP orchards have aroused the increasing attention of researchers in the agricultural robot field [4], [5]. Following this idea, in this paper, we focus on the investigation of the critical control strategy of harvesting robots in SNAP orchards, which is characterized by fast approaching, dynamic tracking and robust to model parameters.

One of the distinct characteristics of SNAP orchards is dense growth. It leads to a more significant interaction of adjacent fruits while harvesting. Fruits are prone to be in motion when the branches are pulled or dragged by harvesters, leading to difficulties for robots aligning objects.

Consequently, the possibility of unsuccessful picks increases, and meanwhile the overall harvesting efficiency falls. In conclusion, the capability of robots to handle the dynamic motion of the target fruits is of significance.

For a long time, cameras have been employed in robotic systems to enhance their sensory ability. In the field of agricultural robots, many vision-based robotic control systems are an open-loop structure [6], [7]. Despite the simplicity of the open-loop control, these systems may suffer from excessive positioning errors in outdoor agricultural environments since continuous image feedback is not opted to verify and rectify the position of the robot w.r.t. the fruit.

As an alternative, a visual servoing scheme ensures a better performance with dynamic objects by combining real-time visual feedback and the actuator control [8]. It makes robots capable of updating objects locations while an end-effector moves toward fruit in real-time [9]. [10] presents a hybrid VS controller combining IBVS and PBVS to control the 3D translation of the camera to guarantee exponential regulation of the robot to a target fruit. Due to environmental disturbances, the fruit target could be in motion. To address this problem, [11] proposed an adaptive VS controller for harvesting robots to compensate for unknown dynamics of fruits online, and afterward, [12] presents a finite-time VS controller to improve robustness of a robot system w.r.t. fruit motion.

Although many positive results improve the real-time performance of harvesting robots in practical orchards, there are still technical challenges in this field.

The first one is the modeling of fruit motion. In the existing literature, the fruit motion is formulated by a combination of two second-order spring-mass systems, e.g. Eq.(3) in [11] and is regarded as known dynamics, e.g. Eq.(11) in [12]. Such the hypothesis makes sense in some situations but brings conservativeness that limits its performance in practical application.

The second challenge is the convergence of visual servoing control systems. Many existing papers concentrate on improving quality of stability with various methods, such as exponential stability [10], finite-time stability [11]. The common control objective of the above work, however, is regulating the end-effector to the desired pixel coordinates and desired fruit depth, e.g., Eq.(5) in [12]. In the set-point control, the velocity and trajectory of the end-effector approaching the target cannot be regulated. In many cases, users may want the end-effector to perform a smooth and variable speed when approaching the fruit or to go along a specific path.

¹Tao Li (lit@nercita.org.cn), Quan Qiu (qiuq@nercita.org.cn) and Chunjiang Zhao (zhaocj@nercita.org.cn) are with Beijing Research Center of Intelligent Equipment for Agriculture, Beijing Academy of Agriculture and Forestry Sciences, Beijing, China,

The third challenge is parameter calibration. A typical way to acquire camera parameters is usually by camera calibration which has been extensively discussed in literature [13]. Moreover, both the calibration of systematic kinematic parameters and the robot dynamic parameters are tedious and inconvenient as well, especially for harvesting robotic systems.

Basing on the three challenges mentioned above, in this paper, we investigate a hybrid visual servoing control scheme for harvesting robots in SNAP orchards. The contributions lie in the three aspects. a) We consider the unknown fruit motion by proposing a hybrid visual servoing configuration. In this paper, an eye-in-hand RGBD camera and a fixed RGBD camera are used to provide abundant image features. b) Visual servoing tracking control is investigated. The desired image trajectory is time-varying. It allows the users to define the way of end-effector approaching fruits. c) Non-calibration. With unknown camera extrinsic and intrinsic parameters and robotic dynamic parameters, the proposed VS tracking controller is uncalibrated. Three adaptive laws are also proposed to update unknown parameters online.

II. MODEL FORMULATION

A. Hybrid visual servoing system

For an RGBD camera, the following relationship holds

$$\mathbf{y}_{rgb} = \Omega_{rgb} \mathbf{x}^c, \quad (1)$$

where $\mathbf{x}^c(t) \in \mathbb{R}^3$ denotes the feature point coordinates of the object in Cartesian frame \mathcal{F} of the RGBD camera; $\mathbf{y}_{rgb}(t) \in \mathbb{R}^3$ denotes the camera image coordinates on the image-space, which consists of two pixel positions on the RGB image and the depth value on the depth image; $\Omega_{rgb} \in \mathbb{R}^{3 \times 3}$ denotes the intrinsic parameters matrix of RGBD cameras which satisfies

$$\Omega_{rgb} = \begin{bmatrix} f k_u / z & f k_u \cot \vartheta / z & u_0 / z \\ 0 & \frac{f k_v}{z \sin \vartheta} & v_0 / z \\ 0 & 0 & \mu \end{bmatrix}. \quad (2)$$

For the detail of matrix Ω_{rgb} , please refer to [14], [15]. Here, μ denotes the approximation relationship between the depth measurement and its true value.

Remark 1: It should be noted that depth measuring errors vary with factors including distance and light intensity. Basing on our previous investigation, we note that, in a certain range of distance and illumination, the measurement and the true value of depth subject to a linear mapping and the value of μ is slightly smaller than 1. Such linear mapping μ is merely a local approximation rather than a rigorous analytic expression. Here, we use the local approximation μ in Eq.(2) as an unknown parameter to be adaptively updated online.

In a hybrid VS system, two RGBD cameras are employed for eye-in-hand and eye-to-hand vision and their image coordinates vectors can be defined by \mathbf{y}_{eih} and \mathbf{y}_{fixed} respectively. Likewise, their intrinsic parametric matrices are denoted by Ω_{eih} , Ω_{fixed} .

Once finished mapping feature positions from camera image-space to camera Cartesian-space, the relationships between manipulators and cameras are required. In hybrid VS systems, the following homogeneous transformation holds:

$${}^{eih}\mathbf{T}_{fixed} = {}^{eih}\mathbf{T}_{EE} {}^{EE}\mathbf{T}_{BASE} {}^{BASE}\mathbf{T}_{fixed}, \quad (3)$$

where ${}^{eih}\mathbf{T}_{EE} \in \text{SE}(3)$ denotes the homogeneous transformation matrix from the eye-in-hand camera frame to the end-effector frame; ${}^{EE}\mathbf{T}_{BASE} \in \text{SE}(3)$ denotes the matrix from the end-effector frame to the base frame; ${}^{BASE}\mathbf{T}_{fixed} \in \text{SE}(3)$ denotes the matrix from the base frame to the eye-to-hand camera frame.

By the above transformation, the mapping relation of feature point coordinates $\mathbf{x}^c(t)$ between different camera frames in Cartesian-space can be formulated as follows

$$\mathbf{x}^{eih} = {}^{eih}\mathbf{T}_{fixed} \mathbf{x}^{fixed}, \quad (4)$$

where $\mathbf{x}^{eih}, \mathbf{x}^{fixed} \in \mathbb{R}^4$ are vectors with 4 elements that the 4th element is 1 to align the homogeneous transformation. Also the following mapping relation hold:

$$\mathbf{x}^{eih} = {}^{eih}\mathbf{T}_{EE} \mathbf{x}^{EE}. \quad (5)$$

Generally speaking, the relative pose between the eye-in-hand camera and the end-effector is invariant as well as the eye-to-hand camera and the robot base during the operation of the manipulator.

Substituting Eq.(5) into Eq.(1), one has

$$\mathbf{y}_{eih} = \Omega_{eih} {}^{eih}\mathbf{T}_{EE} \mathbf{x}^{EE} = \mathbf{M}_{eih} \mathbf{x}^{EE}, \quad (6)$$

where $\mathbf{M}_{eih} \in \mathbb{R}^{3 \times 4}$ denotes perspective projection matrix which is invariant.

Differentiating Eq.(6) and combining them, one has

$$\dot{\mathbf{y}}_{eih} = \mathbf{M}_{eih} {}^{EE}\dot{\mathbf{T}}_{BASE} \mathbf{M}_{fixed}^+ \mathbf{y}_{fixed} + \mathbf{M}_{eih} {}^{EE}\mathbf{T}_{BASE} \mathbf{M}_{fixed}^+ \dot{\mathbf{y}}_{fixed} \quad (7)$$

where \mathbf{M}_{fixed}^+ is the pseudo-inverse matrix of \mathbf{M}_{fixed} .

Rewriting Eq.(7), one has

$$\dot{\mathbf{y}}_{eih} = \mathbf{Q}\dot{\mathbf{q}} + \mathbf{J}_v \dot{\mathbf{y}}_{fixed} \quad (8)$$

where $\dot{\mathbf{q}} \in \mathbb{R}^n$ denotes the joint velocity vector; $\mathbf{Q} \in \mathbb{R}^{3 \times n}$ is robot Jacobian matrix, which describes the forward differential kinematics between image-space of eye-in-hand cameras and joint-space of the robot; $\mathbf{J}_v \in \mathbb{R}^{3 \times 3}$ describes the differential kinematic relation between image-space of the eye-in-hand camera and the fixed camera.

Property 1: For a vector $\phi \in \mathbb{R}^{n \times 1}$, the products $\mathbf{Q}\phi$ can be linearly parameterized as follows

$$\mathbf{Q}\phi = \mathbf{Y}(\mathbf{y}_{fixed}, \mathbf{q}, \phi) \theta_k, \quad (9)$$

where $\mathbf{Y}(\mathbf{y}_{fixed}, \mathbf{q}, \phi) \in \mathbb{R}^{3 \times p_1}$ are regressor matrices which consist of the known parameters; $\theta_k \in \mathbb{R}^{p_1 \times 1}$ is a vector which consists of unknown parameters. The number of unknown parameters p_1 varies according to the D-H parameters of the robot.

Property 2: For a vector $\phi \in \mathbb{R}^{3 \times 1}$, the products $\mathbf{J}\phi$ can be linearly parameterized as follows

$$\mathbf{J}\phi = \mathbf{W}(\mathbf{q}, \phi)\theta_m, \quad (10)$$

where $\mathbf{W}(\mathbf{q}, \phi) \in \mathbb{R}^{3 \times p_2}$ are regressoring matrices which consist of the known parameters; $\theta_h \in \mathbb{R}^{p_2 \times 1}$ is a vector which consists of unknown parameters. The number of unknown parameters p_2 varies according to the D-H parameters of the robot.

B. Robotic dynamics

It is well-known that the dynamics of a robot manipulator can be formulated as [16]

$$\mathbf{H}(\mathbf{q}(t))\ddot{\mathbf{q}}(t) + \left(\frac{1}{2}\dot{\mathbf{H}}(\mathbf{q}(t)) + \mathbf{C}(\mathbf{q}(t), \dot{\mathbf{q}}(t)) \right) \dot{\mathbf{q}} + \mathbf{g}(\mathbf{q}(t)) = \tau, \quad (11)$$

where τ is the $n \times 1$ joint input of the manipulator, $\mathbf{H}(\mathbf{q}(t))$ is the $n \times n$ positive-definite and symmetric inertia matrix and $\mathbf{C}(\mathbf{q}(t), \dot{\mathbf{q}}(t)) \in \mathbb{R}^{n \times n}$ is a skew-symmetric matrix such that for any proper dimensional vector ψ ,

$$\psi^T \mathbf{C}(\mathbf{q}(t), \dot{\mathbf{q}}(t)) \psi = 0. \quad (12)$$

On the left side of (11), the first term is inertia force, the second term represents the Coriolis and centrifugal forces, and the last term $\mathbf{g}(\mathbf{q})$ represents the gravitational force. Eq.(11) can be expressed in a linearizing parameterized form and satisfies the following property [17].

Property 3: The dynamic equation of robot manipulator can be expressed as a linear function as follow

$$\mathbf{H}(\mathbf{q}(t))\ddot{\mathbf{q}}(t) + \left(\frac{1}{2}\dot{\mathbf{H}}(\mathbf{q}(t)) + \mathbf{C}(\mathbf{q}(t), \dot{\mathbf{q}}(t)) \right) \dot{\mathbf{q}} + \mathbf{g}(\mathbf{q}(t)) = \mathbf{Y}_d(\mathbf{q}, \dot{\mathbf{q}}, \ddot{\mathbf{q}}(t))\theta_d, \quad (13)$$

where $\xi \in \mathbb{R}^{n \times 1}$, $\mathbf{Y}_d(\mathbf{q}, \dot{\mathbf{q}}, \ddot{\mathbf{q}}(t)) \in \mathbb{R}^{n \times p_3}$ is the corresponding dynamic regressoring matrix and $\theta_d \in \mathbb{R}^{p_3 \times 1}$ denotes the unknown dynamic parameter vector. The number of unknown parameters is denoted as p_3 and the value of p_3 depends on the number of the joint dimensions [18].

III. HYBRID DYNAMIC VISUAL TRACKING CONTROL AND STABILITY ANALYSIS

A. Problem description

In the system of this paper, three prerequisites are considered, summarized as follows.

- The target fruit is in motion w.r.t. the robot base.
- The camera intrinsic and extrinsic parameters and robot dynamic parameters are unknown.
- The desired image state is a dynamic trajectory rather than a static position.

The control objective is to guarantee the end-effector of the robot to track a user-defined desired trajectory approaching a target fruit for finishing harvesting, which can be formulated by

$$\lim_{t \rightarrow \infty} \Delta \mathbf{y}, \Delta \dot{\mathbf{y}} = 0, \quad (14)$$

where $\Delta \mathbf{y} = \mathbf{y} - \mathbf{y}_d$, $\Delta \dot{\mathbf{y}} = \dot{\mathbf{y}} - \dot{\mathbf{y}}_d$ and $(\mathbf{y}_d, \dot{\mathbf{y}}_d, \ddot{\mathbf{y}}_d)$ is the desired image trajectory that is defined in the eye-in-hand RGBD camera. Note that, for the purpose of simplification, hereafter, we remove the subscript "eih" and use \mathbf{y} to be the shorthand of \mathbf{y}_{eih} but keep the subscript "fixed" in $\mathbf{y}_{\text{fixed}}$ to tell apart.

B. Controller design

We first introduce the following reference image velocity

$$\dot{\mathbf{y}}_r = \dot{\mathbf{y}}_d - \lambda(\mathbf{y} - \mathbf{y}_d) - \hat{\mathbf{J}}\dot{\mathbf{y}}_{\text{fixed}}, \quad (15)$$

where λ is a positive constant; $\hat{\mathbf{J}}$ denotes the estimation matrix of \mathbf{J} that satisfies

$$\hat{\mathbf{J}}\phi = \mathbf{W}(\mathbf{q}, \phi)\hat{\theta}_m, \quad (16)$$

where $\hat{\theta}_m$ is the estimation of unknown vector θ_m . By (15), a novel joint-space reference velocity is defined by

$$\dot{\mathbf{q}}_r = \hat{\mathbf{Q}}^+ \dot{\mathbf{y}}_r, \quad (17)$$

where $\hat{\mathbf{Q}}^+$ denotes the pseudo-inverse of estimated Jacobian matrix and $\hat{\mathbf{Q}}$ is derived from

$$\hat{\mathbf{Q}}\phi = \mathbf{Y}(\mathbf{y}_{\text{fixed}}, \mathbf{q}, \phi)\hat{\theta}_k, \quad (18)$$

where $\hat{\theta}_k$ is the estimation of unknown vector θ_k . Note that both $\hat{\theta}_k$ and $\hat{\theta}_m$ are online updated by the adaptive laws that will be proposed later.

Then a sliding vector in joint-space can be constructed as follows:

$$\mathbf{s}_q = \dot{\mathbf{q}} - \dot{\mathbf{q}}_r, \quad (19)$$

Now we are in a position to present the tracking VS controller of this paper

$$\tau = \mathbf{Y}_d(\mathbf{q}, \dot{\mathbf{q}}, \ddot{\mathbf{q}}_r)\hat{\theta}_d - \hat{\mathbf{Q}}^T \mathbf{K}_1 \Delta \mathbf{y} - \mathbf{K}_2 \mathbf{s}_q, \quad (20)$$

where $\mathbf{K}_1, \mathbf{K}_2 \in \mathbb{R}^{n \times n}$ are positive definitely symmetric matrices to be determined and $\hat{\theta}_d \in \mathbb{R}^{p_3 \times 1}$ denotes the estimation of the unknown dynamic parameter vector.

By combining Eq.(9) and Eq.(18), the estimation error of robot Jacobian matrix is

$$\hat{\mathbf{Q}}\dot{\mathbf{q}} - \mathbf{Q}\dot{\mathbf{q}} = \mathbf{Y}(\mathbf{y}_{\text{fixed}}, \mathbf{q}, \dot{\mathbf{q}})\Delta\hat{\theta}_k. \quad (21)$$

Likewise, with Eq.(10) and Eq.(16), one has

$$\hat{\mathbf{J}}\dot{\mathbf{y}}_{\text{fixed}} - \mathbf{J}\dot{\mathbf{y}}_{\text{fixed}} = \mathbf{W}(\mathbf{q}, \dot{\mathbf{y}}_{\text{fixed}})\Delta\theta_m. \quad (22)$$

By combining Eq.(21), Eq.(17) and Eq.(15), one has

$$\hat{\mathbf{Q}}\mathbf{s}_q = \Delta\dot{\mathbf{y}} + \lambda\Delta\mathbf{y} + \Delta\mathbf{J}_v\dot{\mathbf{y}}_{\text{fixed}} + \mathbf{Y}_k(\mathbf{y}_{\text{fixed}}, \mathbf{q}, \dot{\mathbf{q}}, \ddot{\mathbf{q}}_r)\Delta\theta_k. \quad (23)$$

According to Eq.(13), it yields

$$\begin{aligned} & \mathbf{Y}_d(\mathbf{q}, \dot{\mathbf{q}}, \ddot{\mathbf{q}}(t), \ddot{\mathbf{q}}_r)\theta_d - \mathbf{Y}_d(\mathbf{q}, \dot{\mathbf{q}}, \ddot{\mathbf{q}}_r, \ddot{\mathbf{q}}_r)\hat{\theta}_d \\ &= \mathbf{H}(\mathbf{q}(t))\dot{\mathbf{s}}_q + \left(\frac{1}{2}\dot{\mathbf{H}}(\mathbf{q}(t)) + \mathbf{C}(\mathbf{q}(t), \dot{\mathbf{q}}(t)) \right) \mathbf{s}_q \\ & \quad - \mathbf{Y}_d(\mathbf{q}, \dot{\mathbf{q}}, \ddot{\mathbf{q}}_r, \ddot{\mathbf{q}}_r)\Delta\theta_d. \end{aligned} \quad (24)$$

C. Adaptive laws

In the above analysis, the estimation of $\hat{\mathbf{Q}}, \hat{\mathbf{J}}$ and robotic dynamics (13) are used. These estimations can be linearized by Property 1-3 and can be obtained by the estimations of vectors, $\hat{\theta}_k, \hat{\theta}_m, \hat{\theta}_d$. In order to obtain these estimates of the unknown vectors, we present the following adaptive laws:

$$\dot{\hat{\theta}}_d = -\Psi_d^{-1} \mathbf{Y}_d^T(\mathbf{q}, \dot{\mathbf{q}}, \ddot{\mathbf{q}}_r) \mathbf{s}_q, \quad (25)$$

$$\dot{\hat{\theta}}_k = \Psi_k^{-1} \mathbf{Y}_k^T(\mathbf{y}_{\text{fixed}}, \mathbf{q}, \dot{\mathbf{q}}, \ddot{\mathbf{q}}_r) \mathbf{K}_1 \Delta \mathbf{y}, \quad (26)$$

$$\dot{\hat{\theta}}_m = \Psi_m^{-1} \mathbf{W}^T(\mathbf{q}, \dot{\mathbf{y}}_{\text{fixed}}) \mathbf{K}_1 \Delta \mathbf{y}, \quad (27)$$

where Ψ_d, Ψ_k and Ψ_m are positive definite symmetric matrices with proper dimensions.

D. Stability Analysis

Theorem 1: For the visual servoing robotic system described in Subsection III-A, the controller (20) and the adaptive laws (25)-(27) for the visual servoing robotic system can guarantee the asymptotic convergence of the image-space tracking position errors and the velocity errors, namely, $\Delta \mathbf{y}, \Delta \dot{\mathbf{y}} \rightarrow 0$ as $t \rightarrow \infty$.

Proof: Consider a Lyapunov function candidate V in form of

$$V = V_1 + V_2, \quad (28)$$

where

$$\begin{aligned} V_1 &:= \frac{1}{2} \mathbf{s}_q^T \mathbf{H} \mathbf{s}_q + \frac{1}{2} \Delta \mathbf{y}^T \mathbf{K}_1 \Delta \mathbf{y}, \\ V_2 &:= \frac{1}{2} \Delta \theta_d^T \Psi_d^T \Delta \theta_d + \frac{1}{2} \Delta \theta_k^T \Psi_k^T \Delta \theta_k + \frac{1}{2} \Delta \theta_m^T \Psi_m^T \Delta \theta_m. \end{aligned} \quad (29)$$

Substituting the controller (20) into Eq.(13), one gets

$$\begin{aligned} &\mathbf{H}(\mathbf{q}(t)) \dot{\mathbf{s}}_q + \left(\frac{1}{2} \dot{\mathbf{H}}(\mathbf{q}(t)) + \mathbf{C}(\mathbf{q}(t), \dot{\mathbf{q}}(t)) \right) \mathbf{s}_q \\ &\quad - \mathbf{Y}_d(\mathbf{q}, \dot{\mathbf{q}}, \ddot{\mathbf{q}}_r) \Delta \theta_d \\ &= -\hat{\mathbf{Q}}^T \mathbf{K}_1 \Delta \mathbf{y} - \mathbf{K}_2 \mathbf{s}_q. \end{aligned} \quad (30)$$

Differentiating V_1 with respect to time leads to

$$\dot{V}_1 = \mathbf{s}_q^T \mathbf{H} \dot{\mathbf{s}}_q + \frac{1}{2} \mathbf{s}_q^T \dot{\mathbf{H}} \mathbf{s}_q + \Delta \mathbf{y}^T \mathbf{K}_1 \Delta \dot{\mathbf{y}}. \quad (31)$$

Invoking Eq.(12) and left multiplying \mathbf{s}_q^T on both sides of Eq.(30), after simple calculations, one gets

$$\begin{aligned} \dot{V}_1 &= \mathbf{s}_q^T \mathbf{Y}_d(\mathbf{q}, \dot{\mathbf{q}}, \ddot{\mathbf{q}}_r) \Delta \theta_d - \lambda \Delta \mathbf{y}^T \mathbf{K}_1 \Delta \mathbf{y} \\ &\quad - \dot{\mathbf{y}}_{\text{fixed}}^T \Delta \mathbf{J}_v \mathbf{K}_1 \Delta \mathbf{y} - \Delta \theta_k^T \mathbf{Y}_k^T(\mathbf{y}_{\text{fixed}}, \mathbf{q}, \dot{\mathbf{q}}, \ddot{\mathbf{q}}_r) \mathbf{K}_1 \Delta \mathbf{y} \\ &\quad - \mathbf{s}_q^T \mathbf{K}_2 \mathbf{s}_q. \end{aligned} \quad (32)$$

Differentiating V_2 w.r.t. time leads to

$$\begin{aligned} \dot{V}_2 &= \Delta \theta_d^T \Psi_d^T \dot{\hat{\theta}}_d + \Delta \theta_k^T \Psi_k^T \dot{\hat{\theta}}_k + \Delta \theta_m^T \Psi_m^T \dot{\hat{\theta}}_m \\ &= -\Delta \theta_d^T \mathbf{Y}_d^T(\mathbf{q}, \dot{\mathbf{q}}, \ddot{\mathbf{q}}_r) \mathbf{s}_q \\ &\quad + \Delta \theta_k^T \mathbf{Y}_k^T(\mathbf{y}_{\text{fixed}}, \mathbf{q}, \dot{\mathbf{q}}, \ddot{\mathbf{q}}_r) \mathbf{K}_1 \Delta \mathbf{y} \\ &\quad + \dot{\mathbf{y}}_{\text{fixed}}^T \Delta \mathbf{J}_v^T \mathbf{K}_1 \Delta \mathbf{y}. \end{aligned} \quad (33)$$

Then combining Eq.(32) and Eq.(33), one has

$$\dot{V} = -\lambda \Delta \mathbf{y}^T \mathbf{K}_1 \Delta \mathbf{y} - \mathbf{s}_q^T \mathbf{K}_2 \mathbf{s}_q. \quad (34)$$

Because $\lambda, \mathbf{K}_1, \mathbf{K}_2$ are positive, $\dot{V} \leq 0$ can be easily derived according to Eq.(34). It means that the value of V will not accumulate, which means it has upper bound. According to the definition of Lyapunov function candidate V , $\mathbf{s}_q, \Delta \mathbf{y}, \Delta \theta_k, \Delta \theta_d, \Delta \theta_m$ are all bounded. The boundedness of $\mathbf{y}_d, \theta_d, \theta_k, \theta_m$ is known, then we can easily derive the boundedness of $\hat{\theta}_d, \hat{\theta}_k, \hat{\theta}_m, \mathbf{y}$. By Property 1-3, the boundedness of $\hat{\mathbf{J}}, \hat{\mathbf{Q}}$ can be obtained.

From Eq.(15), $\dot{\mathbf{y}}_r$ is bounded due to the boundedness of $\Delta \mathbf{y}, \dot{\mathbf{y}}_{\text{fixed}}$ and $\dot{\mathbf{y}}_d$. Then the boundedness of $\dot{\mathbf{q}}_r$ holds. We can therefore derive that $\dot{\mathbf{q}}, \dot{\mathbf{y}}$ are bounded. Since \dot{V} is differentiable, to check the uniform continuity of \dot{V} , we differentiate \dot{V} as follows:

$$\ddot{V} = -2\lambda \Delta \mathbf{y}^T \mathbf{K}_1 \Delta \dot{\mathbf{y}} - 2\mathbf{s}_q^T \mathbf{K}_2 \dot{\mathbf{s}}_q. \quad (35)$$

By the differential of \mathbf{s}_q and above analysis, it is easy to derive the boundedness of $\dot{\mathbf{s}}_q$. Moreover, by Eq.(35), it is not hard to derive the boundedness of \ddot{V} , which means that \dot{V} is uniformly continuous. Combining with lower the bounded V and the negative semi-definite \dot{V} , we obtain $\dot{V} \rightarrow 0$ as $t \rightarrow \infty$, which leads to $\Delta \mathbf{y} \rightarrow 0, \mathbf{s}_q \rightarrow 0$ as $t \rightarrow \infty$.

According to Barbalet's Lemma, in order to prove $\Delta \mathbf{y} \rightarrow 0$ as $t \rightarrow \infty$, we need to prove the uniform continuity of $\Delta \dot{\mathbf{y}}$. By differentiating (7), the boundedness of $\ddot{\mathbf{y}}$ can be easily derived as well as the boundedness of $\Delta \ddot{\mathbf{y}}$. Finally, the uniform continuity of $\Delta \dot{\mathbf{y}}$ is proved. Equivalently, $\Delta \dot{\mathbf{y}} \rightarrow 0$ as $t \rightarrow \infty$ is proved according to Barbalat's Lemma. ■

IV. EXPERIMENTAL RESULTS

A. Fruits detection platform

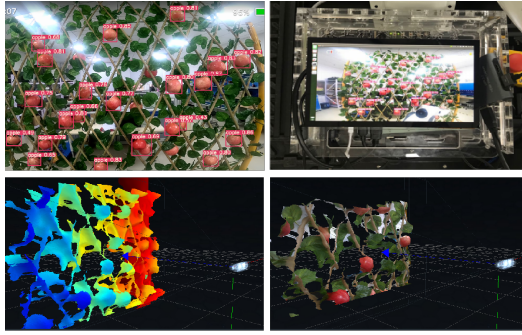
The fruits perception platform consists of two Realsense D435i and NVIDIA Jetson TX2. The in-lab experimental scene simulates the dwarf culture orchards that are with narrow canopy and good visibility.

The image processing system is based on YOLOV5 [19] and DeepSORT [20] algorithm to track fruits in the canopy. The model of the YOLOV5 network has been well-trained by the data set collected in different SNAP orchards. By combined with DeepSORT, the image processing system guarantees that apples can be tracked and marked with identities in RGB frames. The image processing systems acquire good performance in practical orchards, as shown in Fig.1.

B. Harvesting robots control simulation

We use a quasi digital twin method to establish a digital replica of a dwarf culture orchard. To this end, we use MuJoCo (Multi-Joint dynamics with Contact), a physics engine, to facilitate our simulation research.

In this simulation, we model an orchard working environment with two-arm harvesting robots, as shown in Fig.2. The fixed RGBD camera is installed at a metal stand which is immobilized to the wheeled mobile robot and the EIH RGBD camera is mounted at the end-effector. The apples



(a) In-lab test



(b) Orchard test

Fig. 1. Fruits detection experimental results

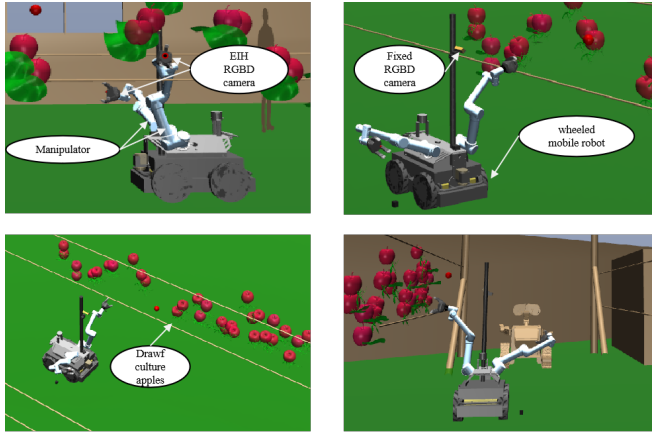
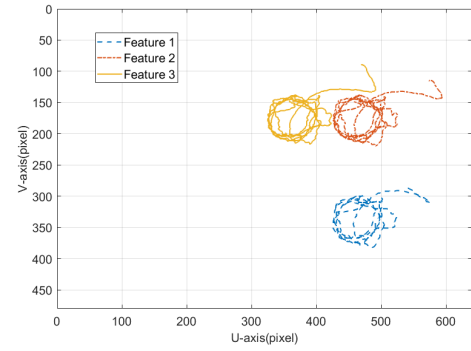


Fig. 2. The harvesting robots working environment based on MuJoCo

are modeled by apple-shaped mesh files and are flexibly connected to different junctions simulating apples hanging on branches. Besides, the apples in the virtual environment are also assigned physical properties, such as gravity, friction, collision et al. The two arms used are UR5 and are modeled by the official urdf files.

Recalling the problem description in subsection III-A, we clarify how the three prerequisites are defined in the simulation. The motions of target fruit w.r.t. the robot base are considered in two ways: circle and rectangle. The circular motion resembles the apple swinging on the branch; the rectangle motion resembles that the harvesting robot is performing search behavior along the fruit wall, where the rectangle motion is caused by the motion of the robot base. Second, the camera intrinsic and extrinsic parameters and



(a) The proposed controller



(b) The reference controller

Fig. 3. Actual image trajectories of end-effector under two control scheme with circular motions of targets

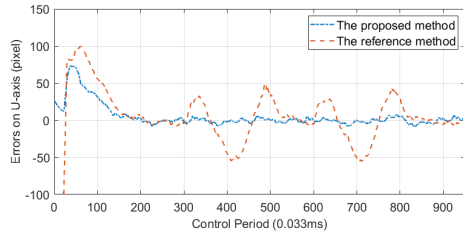
robot dynamic parameters are not used in the controller design even though they can be easily obtained in our simulation. Yet they are not available all the time in practice. Third, the desired image trajectory is defined by a cylindrical spiral in the 3-dimensional image-space of the RGBD camera. Note that in practical harvest, the approaching way along with a cylindrical spiral may be not an efficient one. We use it just for demonstrating the tracking performance better.

Based on the above analysis, the simulations are conducted to verify the tracking performance of the proposed control method with the different motion of target features and with uncalibrated model parameters. To verify the superiority of the proposed hybrid VS configuration, a controller proposed by [21] with EIH configuration is taken as the reference.

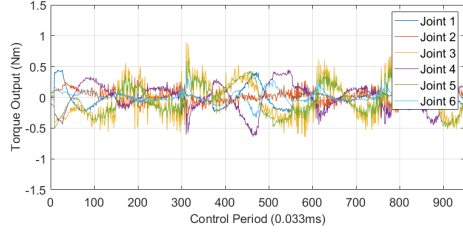
In the simulations, we assume that four reference image features can be observed and tracked by two RGBD cameras.

The circular motion is first considered. In the controller (20) and Jacobian matrices settings, we randomly assign the initial values of the unknown parameters to test the adaption of the proposed method. Fig.3 - Fig.4 demonstrate the results of the simulation. Fig.3 shows that both tracking errors in RGB-image-space and depth-image-space converge to zero well with the proposed controller; in contrast, the convergence of the reference scheme shows unsatisfactory responses. Besides, Fig.4 presents that the actual torque outputs of the proposed controller, which demonstrates that the robot can well track the desired image trajectory approaching the target.

After that a rectangle motion of the robot base w.r.t.

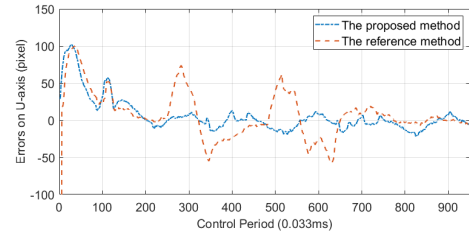


(a) The RGB image errors convergence

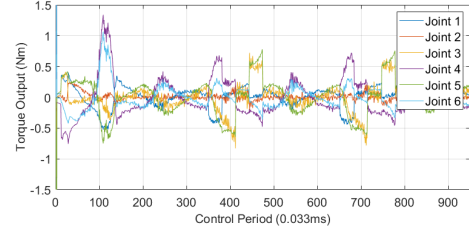


(b) The torque outputs of the proposed controller

Fig. 4. The profiles of image errors and the controller torque outputs of the proposed control method



(a) The RGB image errors convergence



(b) The torque outputs

Fig. 6. The profiles of image errors and the controller torque outputs of the proposed control method

V. CONCLUSIONS

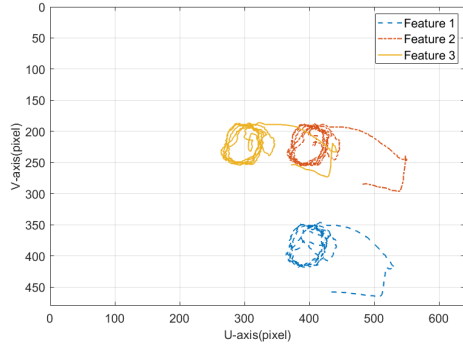
In this paper, we proposed a new hybrid uncalibrated VS control scheme for harvesting robots to track the desired trajectory with the unknown moving feature point w.r.t. the base frame. A rigorous mathematic analysis is given to prove that the proposed controller guarantees the asymptotic convergence of the closed-loop system during the desired trajectory tracking in the presence of the threefold uncalibrated parameters. The performance and superiority of the proposed method have been verified by the comparative simulations.

ACKNOWLEDGMENT

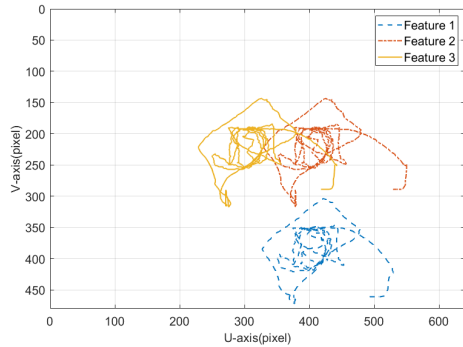
This work was funded by National Science Foundation of China (No.61973040), China Postdoctoral Science Foundation, Postdoctoral Science Foundation of Beijing Academy of Agriculture and Forestry Sciences of China (No.2020-ZZ-001).

REFERENCES

- [1] X. Ling, Y. Zhao, L. Gong, C. Liu, and T. Wang, "Dual-arm cooperation and implementing for robotic harvesting tomato using binocular vision," *Robotics and Autonomous Systems*, vol. 114, pp. 134–143, 2019.
- [2] C. J. Hohimer, H. Wang, S. Bhusal, J. Miller, C. Mo, and M. Karkee, "Design and field evaluation of a robotic apple harvesting system with a 3d-printed soft-robotic end-effector," *Transactions of the ASABE*, vol. 62, no. 2, pp. 405–414, 2019.
- [3] Y. Jiao, R. Luo, Q. Li, X. Deng, X. Yin, C. Ruan, and W. Jia, "Detection and localization of overlapped fruits application in an apple harvesting robot," *Electronics*, vol. 9, no. 6, p. 1023, 2020.
- [4] V. Bloch, A. Degani, and A. Bechar, "A methodology of orchard architecture design for an optimal harvesting robot," *Biosystems Engineering*, vol. 166, pp. 126–137, 2018.
- [5] M. Levin and A. Degani, "A conceptual framework and optimization for a task-based modular harvesting manipulator," *Computers and Electronics in Agriculture*, vol. 166, p. 104987, 2019.
- [6] C. W. Bac, E. J. van Henten, J. Hemming, and Y. Edan, "Harvesting robots for high-value crops: State-of-the-art review and challenges ahead," *Journal of Field Robotics*, vol. 31, no. 6, pp. 888–911, 2014.



(a) The proposed controller



(b) The reference controller

Fig. 5. Actual image trajectories of end-effector under two control scheme with rectangle motions of targets

the target is considered and the comparative simulation is conducted between the proposed method and the reference. The simulating results are given in Fig.5 - Fig.6. The results demonstrate that the proposed controller is capable to regulate the robots approaching targets along with the desired dynamic trajectory even with a rectangle motion of the robot base w.r.t. the targets.

- [7] B. Zhang, Y. Xie, J. Zhou, K. Wang, and Z. Zhang, "State-of-the-art robotic grippers, grasping and control strategies, as well as their applications in agricultural robots: A review," *Computers and Electronics in Agriculture*, vol. 177, p. 105694, 2020.
- [8] F. Chaumette and S. Hutchinson, "Visual servo control. ii. advanced approaches [tutorial]," *IEEE Robotics & Automation Magazine*, vol. 14, no. 1, pp. 109–118, 2007.
- [9] T. Li, H. Zhao, and Y. Chang, "Adaptive cooperative control of networked uncalibrated robotic systems with time-varying communicating delays," *Mathematical Methods in the Applied Sciences*, vol. 42, no. 2, pp. 525–540, 2019.
- [10] S. S. Mehta and T. F. Burks, "Vision-based control of robotic manipulator for citrus harvesting," *Computers and Electronics in Agriculture*, vol. 102, pp. 146–158, 2014.
- [11] S. Mehta and T. Burks, "Adaptive visual servo control of robotic harvesting systems," *IFAC-PapersOnLine*, vol. 49, no. 16, pp. 287–292, 2016.
- [12] S. S. Mehta, M. W. Rysz, P. Ganesh, and T. F. Burks, "Finite-time visual servo control for robotic fruit harvesting in the presence of fruit motion," in *2020 ASABE Annual International Virtual Meeting*. American Society of Agricultural and Biological Engineers, 2020, p. 1.
- [13] J. Heikkilä, "Geometric camera calibration using circular control points," *IEEE Transactions on pattern analysis and machine intelligence*, vol. 22, no. 10, pp. 1066–1077, 2000.
- [14] S. Fuchs and G. Hirzinger, "Extrinsic and depth calibration of tof-cameras," in *2008 IEEE Conference on Computer Vision and Pattern Recognition*. IEEE, 2008, pp. 1–6.
- [15] Y.-H. Liu, H. Wang, C. Wang, and K. K. Lam, "Uncalibrated visual servoing of robots using a depth-independent interaction matrix," *IEEE Transactions on Robotics*, vol. 22, no. 4, pp. 804–817, 2006.
- [16] H. K. Khalil, "Nonlinear systems third edition," *Upper Saddle River, NJ: Prentice-Hall, Inc., 2002*, 2002.
- [17] Y. Su, "Global continuous finite-time tracking of robot manipulators," *International Journal of Robust and Nonlinear Control*, vol. 19, no. 17, pp. 1871–1885, 2009.
- [18] Y. Chang, L. Li, Y. Wang, and K. You, "Toward fast convergence and calibration-free visual servoing control: A new image based uncalibrated finite time control scheme," *IEEE Access*, vol. 8, pp. 88 333–88 347, 2020.
- [19] Z. Zheng, P. Wang, D. Ren, W. Liu, R. Ye, Q. Hu, and W. Zuo, "Enhancing geometric factors in model learning and inference for object detection and instance segmentation," *ArXiv*, vol. abs/2005.03572, 2020.
- [20] N. Wojke, A. Bewley, and D. Paulus, "Simple online and realtime tracking with a deep association metric," in *2017 IEEE International Conference on Image Processing (ICIP)*. IEEE, 2017, pp. 3645–3649.
- [21] T. Li, H. Zhao, and Y. Chang, "Visual servoing tracking control of uncalibrated manipulators with a moving feature point," *International Journal of Systems Science*, vol. 49, no. 11, pp. 2410–2426, 2018.